Dry extrusion of poly(ethylene oxide)-polycarbonate all-solid-state electrolytes for Li-metal batteries: effect of UV-crosslinking on the electrochemical performance

Materials Today Energy 52 (2025) 101947

Contents lists available at ScienceDirect

Materials Today Energy

journal homepage: www.journals.elsevier.com/materials-today-energy/

Dry extrusion of poly(ethylene oxide)-polycarbonate all-solid-state electrolytes for Li-metal batteries: effect of UV-crosslinking on the electrochemical performance

Matteo Gastaldi [a,b], Francesco Gambino [a,b], Hamideh Darjazi [a,b], Alia Jouhara [c], Samuel Malburet [d], Marco Zanetti [e,f], Guido Saracco [a], Giuseppe Antonio Elia [a,b], Claudio Gerbaldi [a,b,*]

[a] GAME Laboratory, Department of Applied Science and Technology (DISAT), Politecnico di Torino, Corso Duca Degli Abruzzi 24, Torino, 10129, Italy
[b] National Reference Center for Electrochemical Energy Storage (GISEL) - INSTM, Via G. Giusti 9, Firenze, 50121, Italy
[c] BlueSolutions, Odet, Ergué Gabéric, CEDEX 9, Quimper, 29556, France
[d] SPECIFIC POLYMERS, 150 Avenue des Cocardières, Castries, 34160, France
[e] Department of Chemistry, SusPlas@Unito – Sustainable Plastic Scientific Hub, University of Turin, Via Pietro Giuria 7, Torino, 10125, Italy
[f] INSTM Reference Centre, University of Turin, Via G. Quarello 15A, Torino, 10135, Italy

ARTICLE INFO

Keywords:
Solid-state battery
Lithium battery
Polymer electrolyte
Poly(ethylene oxide)
Poly(ethylene carbonate)
Solvent-free extrusion

ABSTRACT

All-solid-state lithium-based batteries are amongst the most promising candidates for next-generation energy storage systems. A challenge remains in identifying solid polymer electrolytes (SPE) with high ionic conductivity. Here, we introduce an advanced SPE composed of poly(ethylene oxide) (PEO) and poly(ethylene carbonate) (PEC), fabricated by simple, up-scalable solvent-free extrusion followed by UV crosslinking. This method yields flexible, self-standing electrolytes with remarkable thermal and mechanical stability, ensuring non-flammability and structural integrity, while also being scalable for industrial production. Symmetric Li||Li cells demonstrate outstanding stripping/plating performance across a current density range of 0.025–0.2 mA cm^{-2} at both 40 and 70 °C, exhibiting stable cycling for over 600 h at 0.05 mA cm^{-2} and neglibile Li dendrite growth at 70 °C. Degradation is analysed using nuclear magnetic resonance (NMR) spectroscopy to evaluate the impact of UV crosslinking, while impedance spectroscopy investigates the electronic and ionic transport properties during initial oxidation and reduction processes. The lithium metal polymer cells assembled with a high-loading $LiFePO_4$-based composite catholyte demonstrate near-full specific capacity at low rates (up to 157 mAh g^{-1} at C/5), and show excellent rate capability at 70 °C, paving the way for the design of the next-generation solid-state batteries with enhanced performance.

1. Introduction

Solid-state salt-in-polymer formulations have garnered significant attention as cost-effective, safer, and easier-to-process electrolyte alternatives for lithium metal batteries [1,2]. However, their application has been hindered by degradation phenomena, primarily arising from the high reactivity of lithium at the anode and the interactions with carbon and active materials at the cathode. These factors exacerbate polymer degradation, especially under high-voltage conditions [3–5].

Polyethylene oxide (PEO), first introduced in the 1970s, is one of the most widely used materials for developing solid-state polymer electrolytes (SPEs). Its advantages have been extensively documented in the literature, alongside various strategies and future perspectives for improving its properties [5,6]. However, PEO faces several limitations. Indeed, its electrochemical stability window is relatively narrow, which restricts its compatibility with high-voltage cathodes. This limitation stems from the oxidation of ethylene oxide (EO) units at voltages exceeding 4 V *vs.* Li^+/Li. Furthermore, PEO exhibits low ionic

This article is part of a special issue entitled: Promising Early Career Scientists 2025 published in Materials Today Energy.

* Corresponding author. GAME Laboratory, Department of Applied Science and Technology (DISAT), Politecnico di Torino, Corso Duca Degli Abruzzi 24, Torino, 10129, Italy
E-mail address: claudio.gerbaldi@polito.it (C. Gerbaldi).

https://doi.org/10.1016/j.mtener.2025.101947
Received 1 April 2025; Received in revised form 4 June 2025; Accepted 11 June 2025
Available online 12 June 2025

conductivity at ambient temperatures (≈10^{-8} S cm^{-1}) due to its partially crystalline structure. Additional challenges include incomplete dissociation of lithium salts due to its low dielectric constant, which promotes ion aggregation [1,7,8].

To address the limitations of PEO-based electrolytes, inorganic and ceramic fillers, plasticizers, and additives have been incorporated into homogeneous formulations to reduce crystallinity, enhance ionic conductivity, and improve electrochemical stability [9,10]. However, these modifications present challenges, including increased costs, high interfacial impedance between the electrode and the inorganic solid electrolyte (ISE), and the need for process optimisation to prevent filler aggregation [2,9,11,12]. Alternative approaches include the use of various polymers that can be blended or co-polymerised with PEO, as well as chemical modifications to the polymeric structure, such as functionalisation, crosslinking, or the synthesis and application of single-ion polymers [1,13–19]. Among these strategies, blending and crosslinking are amongst the most widely used and cost-effective methods. They enable tailor-made mechanical and chemical properties for the electrolyte without requiring complex synthesis, additional processing, or significant cost increases [14].

Among the polymers incorporated into PEO formulations, polycarbonates (PCs) have gained popularity due to their favorable electrochemical stability, high lithium transference numbers, enhanced mechanical properties, and weaker coordination with lithium ions. These characteristics ensure efficient lithium salt solubility and facilitate Li^+ ion mobility within the polymer matrix [14]. Polyethylene carbonate (PEC) and polypropylene carbonate (PPC) are commercially available options, valued for their low cost and ease of processing. When blended with PEO and lithium salts such as lithium bis(trifluoromethanesulfonyl)imide (LiTFSI), they produce self-standing, easy to handle electrolytes [14]. PEC, in particular, has been employed as an electrolyte with the addition of $LiNO_3$ and Al_2O_3 as fillers and additives, achieving ionic conductivities in the range of 2–5 × 10^{-5} S cm^{-1} and a lithium transference number of up to 0.56 at 60 °C. To mitigate degradation phenomena, protective layers have been employed to prevent direct contact between PEC and the lithium metal electrode [20]. The copolymerisation of PEC and PEO has been utilised to achieve ionic conductivities of approximately 2 × 10^{-5} S cm^{-1} at 40 °C [21]. Additionally, a double-layer configuration of PEO and PPC has been developed to enhance stability properties: PEO provides stability against lithium metal, while PPC offers flexibility in contact with the lithium iron phosphate (LFP) cathode [22]. However, the primary limitation of PCs is their instability in the presence of strong Lewis acids, such as lithium ions, and weakly coordinating anions like $TFSI^-$ [23].

In this study, we explored the blending of PEO and PEC polymers using a solvent-free approach involving a micro-compounder and extruder, which facilitates the formation of homogeneous polymer matrices [24]. This builds upon our previous work, where we optimised this processing method. To mitigate PEC degradation into its monomer, ethylene carbonate (EC), we introduced a fluorine-substituted benzophenone: having a melting temperature compatible with the extrusion process, it serves as both a hydrogen abstractor and a photoinitiator for UV-induced crosslinking of the polymer matrix [15,25,26]. The optimised electrolyte exhibits enhanced electrochemical performance, with improved stability over time at temperatures up to 70 °C, efficient lithium plating and stripping behavior, and compatibility with LFP catholytes and lithium metal anodes. This configuration delivers excellent charge/discharge profiles at both 70 and 40 °C, even with high-loading LFP catholytes. Degradation phenomena were analysed using nuclear magnetic resonance (NMR) spectroscopy, comparing results from UV-cured and non-UV-cured membranes to reference materials. Findings discussed in the following sessions demonstrate that UV curing reduces PC degradation and produces a non-soluble, stable electrolyte.

2. Experimental

2.1. Materials

Poly(ethylene oxide) - PEO ($M_w = 4 \times 10^5$ g mol^{-1}, CAS 25322-68-3) was obtained from Merck while poly(ethylene carbonate) -PEC (M_w = 2.43 × 10^5 g mol^{-1}, CAS 25608-11-1) was received from Specific Polymers (France). Bis(trifluoromethane) sulfonamide lithium salt (LiTFSI, battery grade, CAS 90076-65-6) as well as 4-4′-difluorobenzophenone (99 %, CAS 345-92-6), which is used as photoinitiator, were provided by Merck. All polymers were dried for 3 days under vacuum at 60 °C and the LiTFSI was dried under vacuum for one day at room temperature, two days at 70 °C, and finally 2 h at 110 °C. All drying procedures were carried out using a B-585 oven (Buchi Glass Drying Oven, Switzerland). All $LiFePO_4$ (LFP) catholyte materials were received by Blue Solutions, produced by a proprietary patented dry process and including PEO:LiTFSI electrolyte as the active binder. Lithium metal was received by BlueSolution with a thickness of 58 μm and used as received. Deuterated dimethyl sulfoxide (d_6-DMSO) was purchased from Merck (99.5 % D, CAS 2206-27-1), stored in an Ar-filled glovebox (M-Braun Unilab, O_2 and H_2O contents < 0.5 ppm), and used as received. Ethyl acetate (EtOAc, CAS: 141-78-6) and acetonitrile (ACN, CAS: 75-05-8) were obtained from Merck and used as received.

2.2. Preparation of the solid polymer electrolytes

All materials were stored and handled in the M-Braun glove box. All the polymer electrolyte formulations were prepared via solvent-free extrusion using a mini-compounder (Haake MiniLab II, Thermo Scientific). The procedure was previously optimised and reported [24]. Briefly, all components were weighed and collected in the glovebox under an inert (Ar) atmosphere and then mixed in the mini extruder under a constant N_2 flux to avoid possible water contaminations. Firstly, one portion of the PEO/PEC formulation was introduced into the extruder, followed by LiTFSI salt (and the 4,4′-difluorobenzophenone as a photoinitiator for the crosslinkable formulation), and then the last part of the PEO/PEC formulation. All components were mixed at 140 °C and 130 rpm for 15 min to ensure good homogeneity and solubilisation of both the salt and the photoinitiator. The resulting formulations were extruded as filaments, then stored under vacuum and transferred into the glovebox. They were used to prepare the truly solid blend polymer electrolytes (namely, PEO-PEC) by hot-pressing them under inert atmosphere at 70 °C and 25 bar (pre-heating the materials for 15 min at 70 °C) to obtain ~10 cm in diameter films having a thickness of about 100 μm. To obtain crosslinked samples (PEO-PEC-UV), the same hot-pressing procedure was exploited, followed by a UV-induced photopolymerization (UV-curing, UV-crosslinking) process at around 70 °C for 3 min on each side under a UV Lamp (DMAX ECE 5000 flood lamps) at 40 mW cm^{-2}. All SPEs underwent another drying step at 40 °C under vacuum for 12 h in the B-585 oven (Buchi Glass Drying Oven, Switzerland) and then were stored in the glove box. The ratio between [EO] and [Li^+] units was fixed at 20:1, reported as optimal in terms of ionic conductivity at high temperatures and reduced stickiness [27], while the best ratio (1:1) among PEO and PEC, previously reported [24], was used here for the polymer fraction. The two types of samples appear as quasi-transparent and homogeneous membranes. The non-UV-cured and UV-cured (crosslinked) SPE samples are labeled as PEO-PEC and PEO-PEC-UV, respectively.

2.3. Characterization

The thermal stability was measured by thermogravimetric analysis (TGA, Netzsch TG 209 F3). The analysis was conducted between 25 and 600 °C under a nitrogen atmosphere (N_2 flux of 100 mL min^{-1}, heating ramp of 10 °C min^{-1}). $T_{d5\ \%}$ was taken as a reference value to determine the temperature at which the sample loses 5 % of the initial weight.

Differential scanning calorimetry (DSC, Netzsch 214 Polyma Equipment) was carried out to evaluate the glass transition temperature (T_g), in the −50/+90 °C temperature range, heating rate of 10 °C min^{-1} under flowing nitrogen (40 mL min^{-1}). The crystallinity degree was calculated as described in Equation (1), using the value of 205 J g^{-1} as melting enthalpy (ΔH_m^0) for 100 % crystalline PEO [28,29].

$$Crystallinity\ (\%) = \frac{\Delta H_m}{\Delta H_m{}^0} * 100 \quad \text{[Eq. 1]}$$

Dynamic mechanical analysis (DMA) was performed on a Q800 V20.24 Build 43 in the −60/+60 °C temperature range with a heating ramp of 3 °C min^{-1}. Before analysis, the samples were placed in a climatic chamber with 50 % humidity and a temperature of 23 °C. A strain of 0.2 % and a preload of 0.01 N were applied and the ramp of temperature was 2 °C min^{-1}. To carry out this analysis, the specimen was cut into 30 × 0.6 mm strips with a thickness of around 150 μm.

The gel content was calculated to evaluate the percentage of non-crosslinked polymer chains still present after UV-curing. The sample (around 0.65 g) was weighed, closed in a metal grid (500 mesh), and soaked in 50 mL of EtOAc for 1 h under stirring at room temperature. Then, the solvent was changed with another 50 mL of fresh EtOAc and kept for 24 h under stirring at room temperature before the third extraction with another 50 mL of fresh solvent for 3 h. The sample was recovered and dried in a vacuum oven until constant weight. The same procedure was repeated on the same sample using acetonitrile (ACN) as solvent. The gel content was evaluated according to Equation (2).

$$Gel\ Content\ (\%) = \frac{w_d}{w_i} * 100 \quad \text{[Eq. 2]}$$

where w_d is the weight after drying and w_i is the initial weight.

For electrochemical characterisations, all polymer electrolytes under study were sandwiched into laboratory-scale ECC-Std electrochemical test cells (EL-Cell, Germany). The ionic conductivity was determined by electrochemical impedance spectroscopy (EIS), using a VMP-3 research-grade multichannel potentiostat/galvanostat with frequency response analyser for high-end EIS measurements (Biologic, France). A membrane disk of 16 mm in diameter, with a thickness of about 150 μm, was sandwiched between two stainless-steel (SS-316) blocking electrodes in a SS||electrolyte||SS configuration. For each SPE, the thickness was accurately measured before and after tests using a precision micrometer (Mitutoyo). EIS data were recorded on the VMP-3 in a frequency range of 0.1 Hz–1 MHz by applying a sinusoidal voltage of 20 mV at various temperatures (0–80 °C) and storing the cells in an environmentally controlled climatic chamber (MK 53 E2 from BINDER, Germany). The cells were kept for 100 min at each temperature with intervals of 10 °C for proper thermal equilibration. Nyquist plots were analysed using the Biologic EC-Lab® advanced software for electrochemical research. The ionic conductivity was determined accordingly to Equation (3):

$$\sigma_i = D/AR \quad \text{[Eq. 3]}$$

where D represents the thickness (cm), A the area (cm^2), and R (Ω) the total resistance of the electrolytes under study.

The electrochemical stability at anodic voltages (oxidation) was evaluated by linear sweep voltammetry (LSV) in the range from the open circuit voltage (E_{ocv}) to 6.0 V with a scan rate of 0.1 mV s^{-1} and fixing 5 μA cm^{-2} as the current threshold to detect the starting of degradation. Test cells were assembled by simply sandwiching the materials in a Li||electrolyte||carbon-coated Al (CC-Al) configuration for LSV and connected to the VMP3 potentiostat/galvanostat for analysis.

The lithium-ion transference number (t_{Li}^+) was determined using a combination of direct current (DC) polarization and alternating current (AC) impedance methods. The AC impedance spectra before and after polarization were obtained via EIS [30]. The transference number was calculated using Eq. (4):

$$t_{Li^+} = \frac{I_s(\Delta V - I_0 R_0)}{I_0(\Delta V - I_s R_s)} \quad \text{[Eq 4]}$$

where R_0 is the impedance resistance before polarization. R_s is the impedance after DC polarization. I_0 is the initial current, I_s is the final current after polarization, and ΔV represents the applied polarization voltage (20 mV).

Lithium plating/stripping tests were performed at different temperatures in symmetrical Li||electrolyte||Li configuration. At 40 °C, the delivered capacity was maintained at 0.20 mAh, corresponding to a constant current of 0.025 mA cm^{-2} applied for 8 h during plating and 8 h during stripping. The rate-dependent experiment was performed by varying the current density between 0.025, 0.050, 0.100, and 0.200 mA cm^{-2}. At 70 °C, the plating/stripping tests were carried out with a fixed capacity of 0.2 mAh (*viz.*, 0.025 mA per 8 h in plating and 8 h in stripping). Also at this temperature, the current density was varied between 0.025, 0.050, 0.100, and 0.200 mA cm^{-2} for the rate-dependent experiment. This latter configuration was also employed for long-term lithium plating/stripping cycling experiments.

To test the practical application potential in real cell configuration of the SPEs under study, lithium metal cells were assembled in a Li||electrolyte||LFP (high-loading catholyte ~10 mg cm^{-2}) configuration connected to an Arbin BT2000 battery tester for galvanostatic cycling tests at different temperatures and current regimes. To evaluate the degradation process of the SPE under study, cells were disassembled in the glovebox after cycling. To compare results, cells underwent the same preparation procedure, the same cycling parameters as well as the same cycling time, until the PEO-PEC sample short-circuited. For NMR analysis, pristine electrolytes were soaked for 24 h in d_6-DMSO. The same procedure was used for analysing samples after galvanostatic cycling. The NMR of all reference materials was obtained by dissolving around 5 mg of each sample in the same deuterated solvent. All spectra are referred to the peak of the d_6-DMSO at 2.50 ppm. Nuclear magnetic resonance ^{1}H NMR (600 MHz) experiments were conducted using a JEOL ECZ-R instrument (^{1}H operating frequency 600 MHz). EIS measurements were conducted for the Li||electrolyte||LFP (catholyte) configuration over the frequency range of 100 mHz to 100 kHz. The bias potential values were scanned in potentiostatic steps of 50 mV, with an equilibration time of 2 h for each step, during the initial oxidation and reduction. All measurements were performed at a temperature of 70 °C.

3. Results and discussion

3.1. Thermomechanical characterization

Thermal stability was tested to investigate the upper temperature limit at which these developed electrolytes can be applied without undergoing degradation phenomena. Thermogravimetric analysis (TGA) was conducted in an inert atmosphere, simulating the working conditions of the battery, for both the PEO-PEC and PEO-PEC-UV membranes. From the comparison between the two thermograms (Fig. S1), the $T_{d5\ \%}$ increased by around 15 °C after crosslinking, thanks to the new covalent bonds linking the polymer chains. In both cases, the degradations start at temperatures around 200 °C, which are usually not reached under standard operation. These results agree with the reported data [21] for non-extruded materials and demonstrate that no degradations or damage to the polymeric material in the extrusion process took place. As reported in a previous work [24], TGA analysis of pure PEO and PEC compounds confirms that both materials exhibit thermal stability up to 200 °C, even in the presence of lithium salt.

Differential scanning calorimetry (DSC) was performed to evaluate the crystallinity degree of the SPEs under study. It is commonly known that crystalline regions should be avoided to enhance ionic conductivity in the polymer network [16,31,32]. Crosslinking is a suitable method to reduce or even eliminate crystalline regions that hinder ionic

conductivity while simultaneously enhancing mechanical properties [12,33]. As shown in Fig. 1a for PEO-PEC, the presence of a melting peak in a range of 40–60 °C suggests the presence of crystalline regions, around 8 % (calculated from Eq. (1)). Moreover, the presence of two distinct T_g peaks at −39.9 and 22.2 °C, respectively, points out the lithium salt effect in increasing the T_g for PEO [34,35] without affecting that of PEC, as well as the limited solubility of the two polymers. Indeed, the presence of two different T_g values, shown in both thermograms in Fig. 1a and b, highlights the non-miscibility of the two polymers, which remain as two different phases that cannot be distinguished by the naked eye nor with SEM pictures, as reported in a previous work [24]. For PEO-PEC-UV, instead, the absence of any melting peak in Fig. 1b reflects the crosslinking effect in preventing crystallisation , making the sample completely amorphous and revealing only the two different T_g values of PEO and PEC. For comparison, the DSC of pure PEO with LiTFSI at a fixed [EO]:[Li^+] ratio of 20:1 is shown in Fig. S2a [24].

Dynamic mechanical analysis (DMA) was carried out to evaluate the mechanical properties before and after UV-curing (Fig. 1c and d). The presence of two distinct peaks in the E″ curves confirms the immiscibility of PEO and PEC, as discussed in the DSC measurements. The first transition, at around −30 °C, corresponds to the T_g of PEO, while the second, at 20 °C, corresponds to that of PEC. The increase in the T_g value from pristine PEO (around −60 °C) is related to the addition of LiTFSI that induces coordination among the Li^+ cations and the PEO chains,resulting in a more rigid structure [36]. The resulting moduli of the polymers above 40 °C are rather low to ensure good mechanical properties and avoid/limit the lithium dendrite formation, but high enough to confer handleability to the SPE. For comparison, the DMA of pure PEO with LiTFSI at a fixed [EO]:[Li^+] ratio of 20:1 is shown in Fig. S2b [24]. To further investigate the crosslinking procedure (Fig. 1d), the gel content analysis was carried out by soaking the samples in two different solvents, EtOAc and ACN, which were chosen to evaluate the reported solubility of the two polymers. Indeed, while PEC is soluble in the former (as reported in the Technical Data Sheet provided by the supplier), PEO is soluble in the latter, as reported in the literature [37]. As a result, after soaking the sample in EtOAc and drying it to constant weight, 97.9 % of the polymer remains undissolved, while 94.1 % remains after ACN soaking. Part of the weight loss is related to the salt and the photoinitiator included in the formulation, meaning that the crosslinking procedure is effective in covalently linking the polymer chains, trapping part of the lithium salt and the photoinitiatorwithin the matrix. In contrast, by applying the same procedure to the PEO-PEC results in its

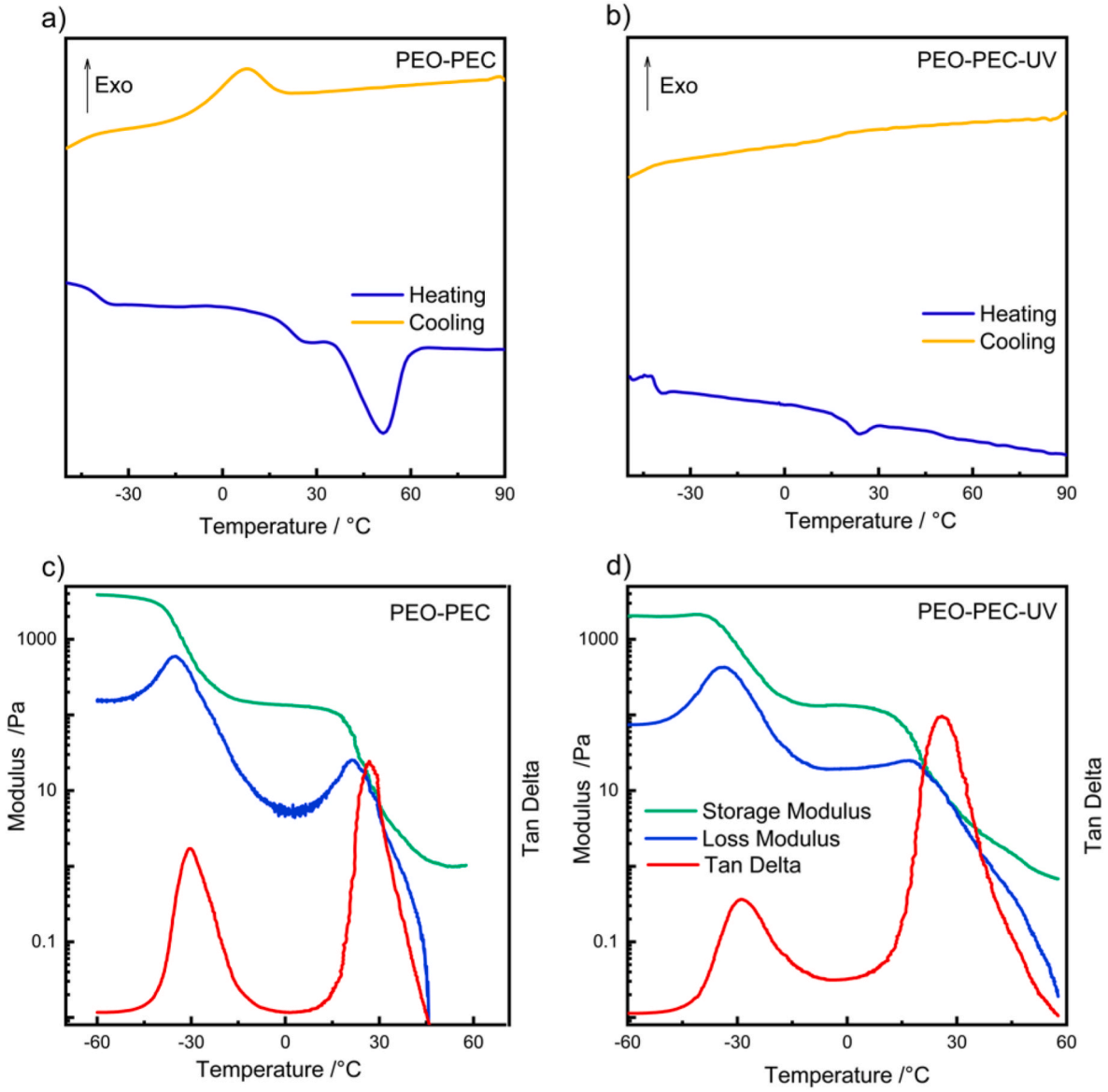

Fig. 1. DSC thermograms of PEO-PEC (a) and PEO-PEC-UV (b), and DMA curves of PEO-PEC (c) and PEO-PEC-UV (d) membranes.

complete dissolution.

3.2. Ionic conductivity and electrochemical characterization

The ionic conductivity was measured from 0 to 80 °C to assess the effect and influence of the introduction of PEC and crosslinking onto materials properties. As shown in Fig. 2a, pure PEO shows a characteristic change in slope around 50–60 °C, corresponding to the melting of its crystalline domains. In contrast, pure PEC shows very low conductivity, even at 80 °C, and becomes undetectable below 40 °C. A less pronounced slope change is observed for PEO-PEC, with an even smoother curve for PEO-PEC-UV. These results confirm the reduction in crystalline regions from pure PEO to the fully amorphous, PEO-PEC-UV sample. However, a slight reduction in the conductivity values is observed for both PEO-PEC and PEO-PEC-UV at temperatures above 60 °C; it is attributed to the presence of PEC, which has lower ionic conductivity. Conversely, between 50 and 0 °C, PEC enhances the electrolyte conductivity due to its ability to dissolve lithium salt without forming stable complexes that would otherwise hinder chain mobility. As a result of reduced chain mobility in the PEO-PEC-UV sample, the ionic conductivity at 70 °C decreases from 8.5×10^{-4} S cm^{-1} for the pristine PEO to 4.2×10^{-4} S cm^{-1} for the PEO-PEC sample, and further to 1.8×10^{-4} S cm^{-1} for PEO-PEC-UV, which is a reasonably high value for a truly solid crosslinked polymer electrolyte.

Based on the ionic conductivity results, two different temperatures (i.e., 40 and 70 °C) were selected to evaluate the electrochemical performance, also investigating the effect of crosslinking, and assessing the thermal stability of the SPE. The electrochemical stability window (ESW) was tested to determine the applicability of these materials as SPEs in lithium metal cells [38,39]. Linear sweep voltammetry (LSV) was employed to evaluate the potential at which possible degradation of the polymer material occur (Fig. 2b). At both temperatures, no significant difference between the PEO-PEC and PEO-PEC-UV samples is detected, with onset potentials of ~ 4.6 V and 4.3 V at 40 °C and 70 °C, respectively, considering a threshold fixed at 5 μA cm^{-2}. While a slight reduction in the oxidation stability is noted as the temperature increases to 70 °C; however, the membranes still exhibit suitable stability for LFP cathodes. For comparison, the ESW vs. oxidation (anodic) of PEO and PEC with LiTFSI at a fixed [EO]:[Li$^+$] ratio of 20:1 is shown in Fig. S3 [24].

The Li$^+$ transference number (t_{Li}^+) reflects the proportion of charge carried by lithium ions and plays a crucial role in controlling the deposition morphology of lithium metal. As shown in Fig. S4, the t_{Li}^+ of the PEO-PEC-UV electrolyte was determined using the Bruce–Vincent–Evans method. The obtained t_{Li}^+ value is 0.47, which is higher compared to standard PEO-LiTFSI SPE and expected after addition of PEC, also accordingly to previously reported values [40].

3.3. Compatibility with the lithium metal electrode

The stability and compatibility of the SPEs at the interface with lithium metal electrodes were investigated through galvanostatic lithium plating/stripping experiments performed at 40 and 70 °C for both PEO-PEC and PEO-PEC-UV. At 70 °C, PEO-PEC fails to sustain even the first plating and stripping cycle (Fig. S5). In contrast, the crosslinked PEO-PEC-UV withstands testing under the same cell configuration with progressively increasing current densities from 0.025 to 0.2 mA cm^{-2} at both temperatures (Fig. 3a and b). At 40 °C, the electrolyte shows good cycling reversibility up to 0.1 mA cm^{-2}, with a maximum overpotential of 0.4 V. When the current is increased to 0.2 mA cm^{-2}, the overpotential exponentially increases; however, no short circuit occurs (Fig. 3a). The PEO-PEC-UV membrane demonstrates improved rate performance for lithium plating/stripping at 70 °C. As the current density increases from 0.025 to 0.100 mA cm^{-2}, the overpotential rises from 0.02 V to 0.11 V (Fig. 3b). Stable cycling is still achieved at 0.2 mA cm^{-2}, with the overpotential increasing to 0.3 V. To ensure the long-term durability and safety of PEO-PEC-UV in lithium metal cells, a prolonged plating/stripping test was conducted at a constant current density of 0.050 mA cm^{-2} (Fig. 3c). Throughout the test (total fixed capacity of 0.2 mAh for each plating and stripping step), no significant rise in overpotential is observed compared to the initial value, nor are there any sudden or unexpected current spikes or drifts accounting for uneven dendrite formation. During the first hundred hours, a slight decrease in overpotential is observed, likely due to the stabilisation process of the cell. Afterward, the cell shows stable behaviour for 600 h, with an overpotential of 0.025 V (Fig. 3c).

3.4. Performances of SPE-based lithium metal batteries

The applicability of the resulting PEO-PEC-UV sample in lithium

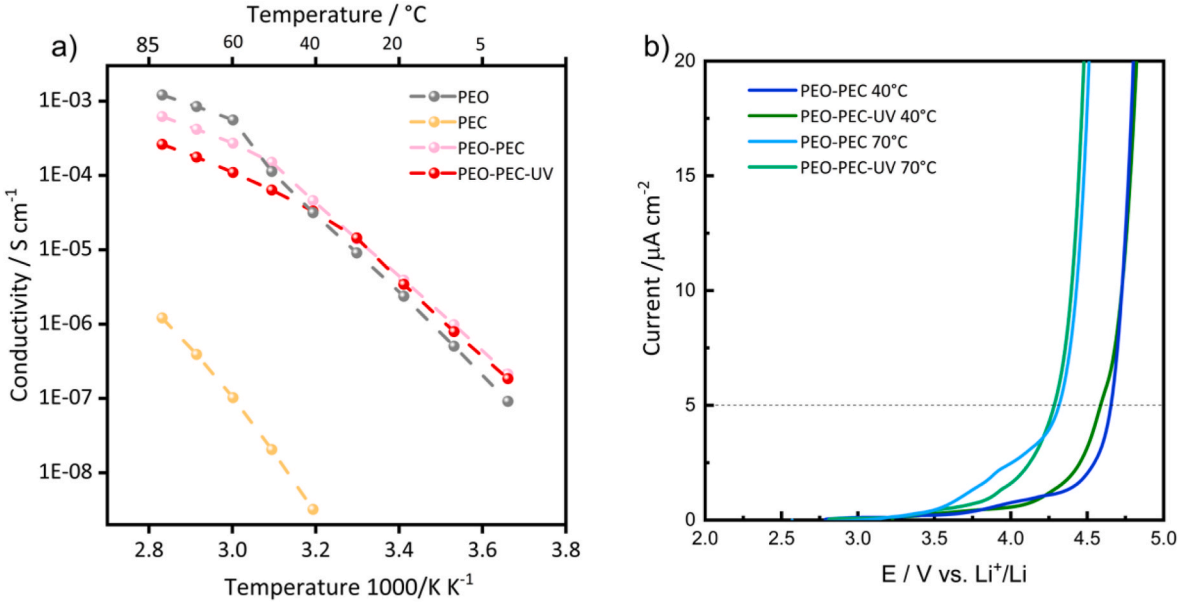

Fig. 2. Ionic conductivity of pure polymers, PEO-PEC, and PEO-PEC-UV (a), maintaining the same [EO]:[Li$^+$] ratio across all formulations. ESW in oxidation for both PEO-PEC and PEO-PEC-UV at 40 and 70 °C (b).

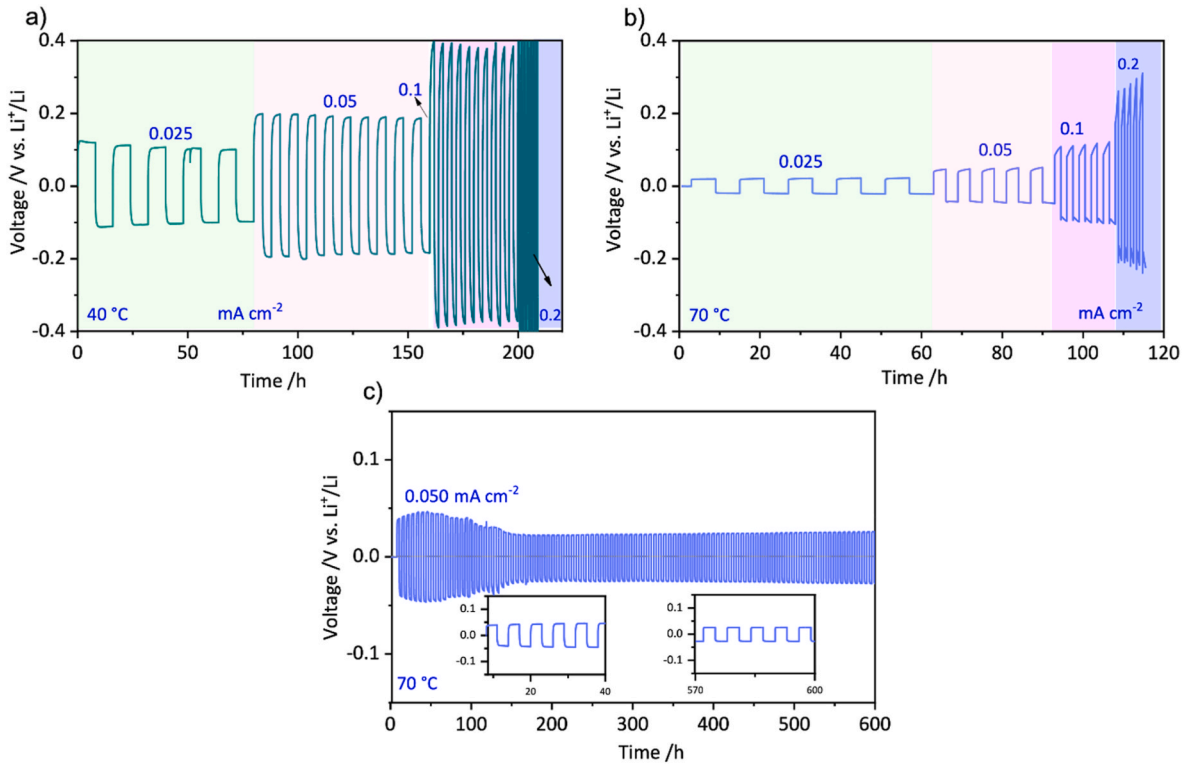

Fig. 3. Voltage profiles of the symmetric Li cells nostatic plating/stripping test at various current densities: (a) at 40 °C and (b) at 70 °C. Cycling performances of Li/Li symmetric cell at 0.050 mA cm^{-2} at 70 °C.

metal cells was tested with a LFP-based electrode, in a high-loading (around 10 mg cm^{-2}) catholyte configuration. Fig. 4a shows the discharge capacity as a function of the current density at C/20, C/10, C/5, and back to C/20 in the 2.5–4.0 V vs. Li^+/Li voltage window. During the initial cycle, the cell exhibits a charge capacity of 172.5 mAh g^{-1} with a Coulombic efficiency (CE) of 89.5 %. However, after few cycles, the capacity stabilises around 168.6 mAh g^{-1} with a CE of 99.9 %. These results indicate that the cell delivers excellent rate performance at all C-rates, maintaining the same specific charge capacity when the current is increased to C/10, with a CE of 99 %. At C/5, the capacity slightly drops to 157 mAh g^{-1} with a CE of 98–99 %. Meanwhile, the increase in polarization voltage at different current densities, even after cycling up to 40 cycles, as shown in Fig. 4b and c, is negligible, further demonstrating its good cycling reversibility. The promising rate performance of the Li||PEO-PEC-UV||LFP cell with a high-loading cathode can be attributed to the high Li^+ conductivity and transport number of the crosslinked SPE, along with excellent electrode-electrolyte compatibility, which promotes homogeneous Li^+ deposition and stable SEI layer formation.

Further measurements were performed on PEO-PEC-UV in lithium-metal cells, which were tested with an LFP-based electrode in the high-loading catholyte configuration at a lower temperature (40 °C), as shown in Fig. S6. As can be observed, the cell exhibits an initial charge capacity of 165.5 mAh g^{-1} with an initial CE of 77.7 % at C/50. After activation and stabilisation of the electrode-electrolyte interface, the capacity remains stable with a CE of 99 % at both C/50 and C/20. However, the cell shows a capacity drop at C/10 and a slight decrease when returning to C/20 after 40 cycles. It is worth noticing that we were unable to achieve stable cycling with a pristine PEO-LiTFSI under similar conditions using the thick, high-loading LFP-based, thus related results are not shown here. From these results, we can conclude that the crosslinking enhances the mechanical properties, limiting the lithium dendrites formation and growth, thus enabling stable cell cycling. Moreover, the electrochemical behaviour observed at both temperatures indicates that PEO-PEC-UV remains stable without showing depolymerisation, even when in contact with lithium metal or in the presence of lithium salt. A deep investigation of the degradation and depolymerisation process is described in the following section.

3.5. *Degradation of the polymer electrolyte*

Polycarbonates are known to depolymerise into their monomers in the presence of lithium ions, lithium metal, and high temperatures [41]. The degradation of PEC leads to the production of EC, a liquid monomer above 40 °C, which can dissolve the polymer network, allowing for direct contact between the lithium and the cathode, causing short-circuiting. This degradation explains the poor performance of PEO-PEC polymer electrolyte membranes. To shed more light on this phenomenon, cells were disassembled in a glove box after cycling for visual inspection of the different components, particularly the electrolyte, and following NMR analysis for characterization of any degradation phenomena (Fig. 5 a-d). Fig. 5a and b show the aspect of PEO-PEC and the PEO-PEC-UV SPEs in symmetrical Li||Li cells after the lithium plating/stripping tests. Both cells underwent the same testing procedure: cycling at 70 °C, and stopping at the same time when the cell with the PEO-PEC short-circuited (indeed, the one with PEO-PEC-UV was still operating properly). As shown in Fig. 5a, PEO-PEC becomes liquid after cycling, indicating depolymerisation into EC monomer. In contrast, PEO-PEC-UV (Fig. 5b) maintains its solid form, demonstrating enhanced mechanical robustness and stability over temperature. Upon NMR analysis, the PEO-PEC sample before cycling (Fig. 5c) shows peaks related to PEO and PEC. After cycling, PEC degrades into EC monomers, which, at 70 °C, act as a solvent and dissolve the polymer matrix. For PEO-PEC-UV (Fig. 5d), the UV crosslinking process prevents complete dissolution of the polymer network; indeed, only a small amount of PEC that is not crosslinked is degraded to EC. Notably, while the crosslinking maintains the membrane integrity, the resulting small amount of EC produced is encompassed in the crosslinked polymer matrix, acting as a plasticiser and enhancing lithium-ion mobility.

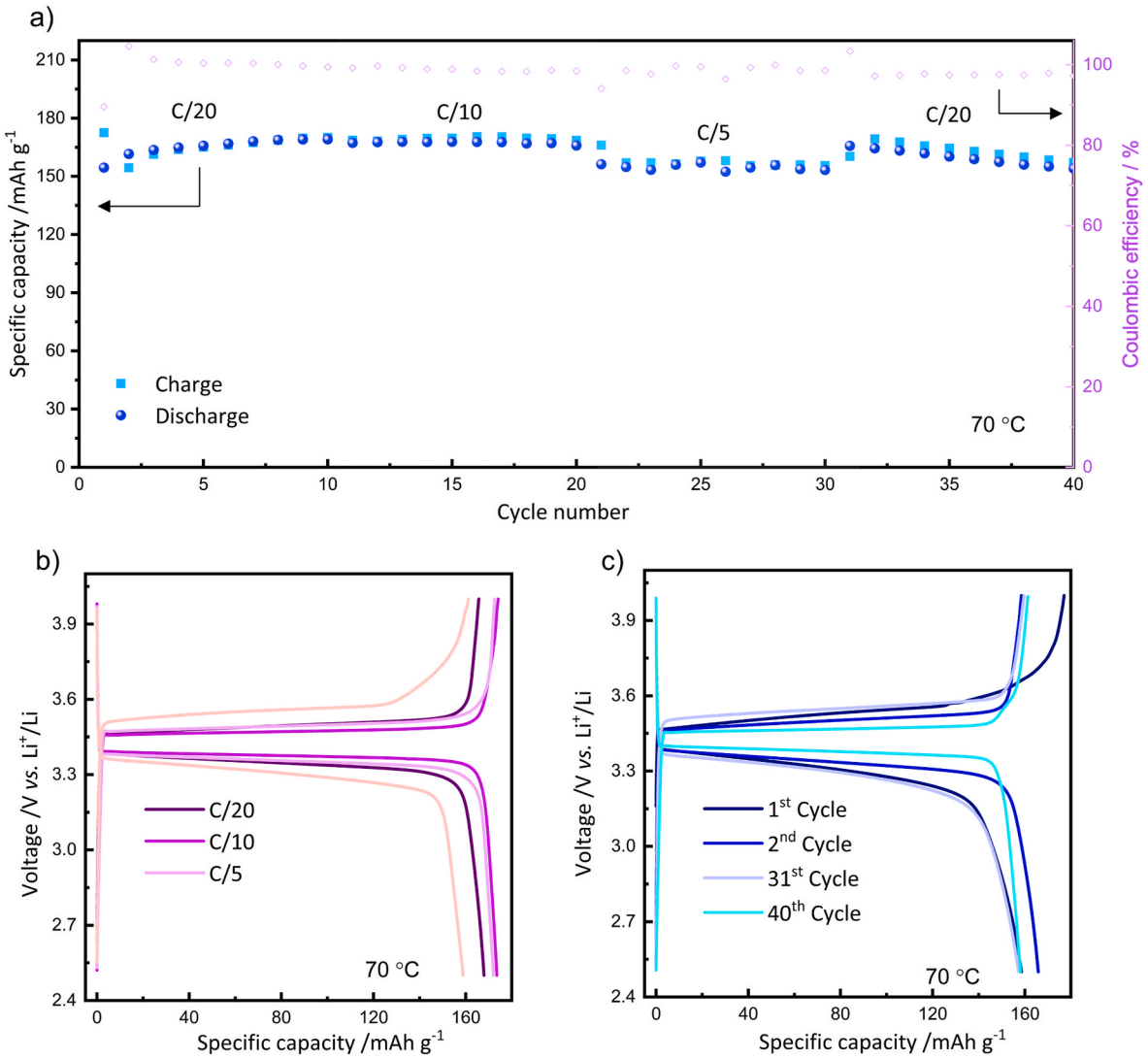

Fig. 4. Rate capability of Li||PEO-PEC-UV||LFP at 70 °C (a) and the corresponding voltage distribution curves upon charge and discharge (b, c).

These results are further supported by the ATR-FTIR spectra shown in Fig. S7, which compare the spectra of PEO-PEC-UV before and after lithium plating/stripping cycles with those of the pristine materials containing LiTFSI. The single peak at 1737 cm^{-1} is associated with the C=O stretching of carbonate groups in PEC-LiTFSI, while the same reflection is split in liquid EC-LiTFSI. As expected, the crosslinked PEO-PEC-UV sample before cycling only shows the features of PEC in the 1700–1800 cm^{-1} range. After cycling, a distinct split EC signal also emerges which overlaps with the peak at 1737 cm^{-1} of PEC, accounting for only partial degradation of PEC to EC, consistent with the NMR results.

3.6. *Interfacial stability of the solid polymer electrolytes*

To better understand the kinetics of the charge and discharge processes, EIS measurements were conducted by collecting a series of spectra during the oxidation and reduction phases of the initial cycle, with bias potentials increased in small steps of 50 mV across the potential range of 2.5–4.0 V. These measurements were performed at 70 °C using Li||PEO-PEC-UV||LFP catholyte cell. Fig. 6 a,b show selected sequences of Nyquist plots acquired for the cell. When the cell is within the voltage range of 2.5 V ≤ E ≤ 3.8 V, the following contributions to the overall impedance can be identified in the Nyquist plots and assigned to specific steps in the electronic/ionic transport, from high to low frequencies: (i) the intercept with the real axis represents the ionic resistance of the SPE layer (R_s), which depends on the ionic conductivity and thickness of the layer; (ii) two overlapping arcs in the high-to-middle frequencies are caused by the interfacial resistances (R_{int}), which may either correspond to ion or electron transfer, depending on the type of interface; (iii) the Warburg diffusion element (W) is evidenced by the sloped line at the lowest-frequency limit, describing the diffusion of Li^+ ions to a blocking electrode [42–44]. However, when the voltage range is 3.8 V ≤ E ≤ 4.0 V, the shape of the curve in the low-frequency region of the Nyquist plots indicates the composite nature of the cathode, which can be accurately described using a Transmission Line Model (TLM) [45]. To capture the response at very low frequencies, a Warburg open element (W_O) is incorporated in series with the TLM. As a result, the spectra during charge and discharge were fitted with two distinct equivalent circuits, as shown in Fig. 6c and d. To account for deviations from ideal behavior caused by electrode inhomogeneity or roughness, all capacitance (C) elements were substituted with constant-phase elements (Q) during the fitting procedure [46]. This fitting was performed using the RelaxIS software by rhd Instruments. The interfacial resistances within the cell (catholyte/SPE/Li) hinder the transport of Li^+ and electrons (Fig. 6f). The composite cathode consists of the cathode active material (CAM), a carbon additive, and the catholyte. The catholyte often contains a solid polymer analogous to the one used in the SPE. The TLM used follows the approach described by

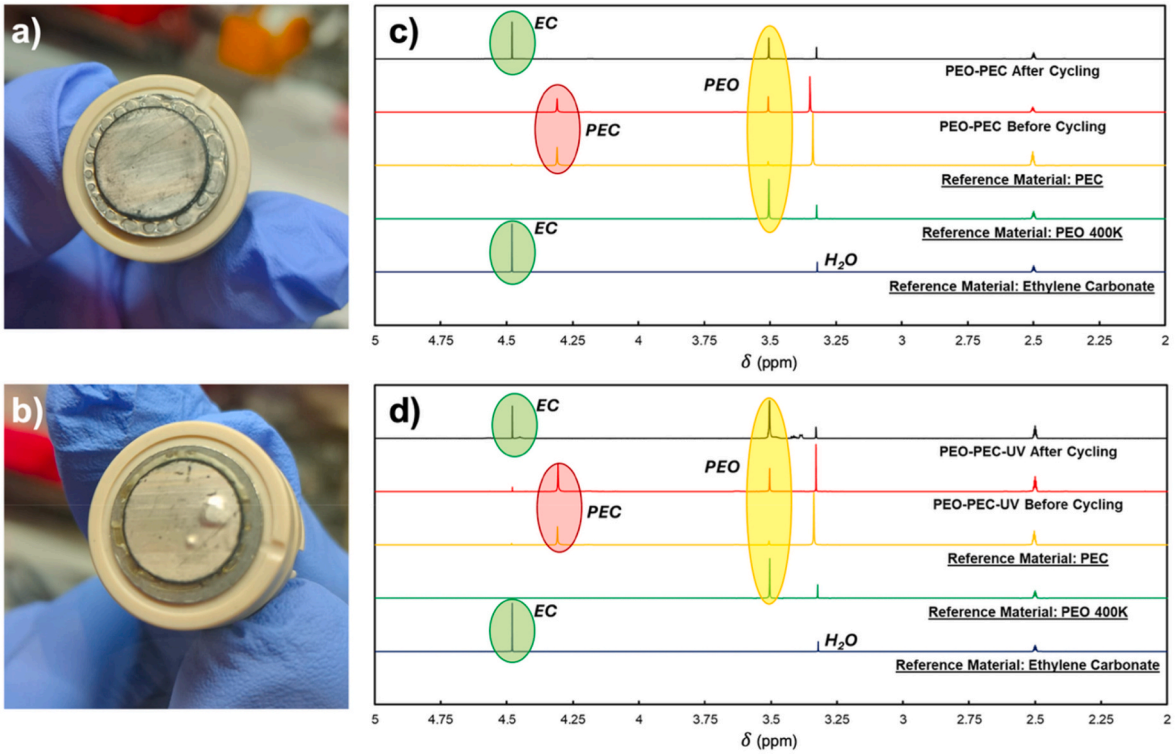

Fig. 5. Pictures of PEO-PEC (a) and PEO-PEC-UV (b) polymer electrolyte membranes after lithium plating/stripping cycling (cells were disassembled after the PEO-PEC cell short circuited); corresponding NMR spectra of PEO-PEC (c) and PEO-PEC-UV (d).

Wurster et al. [42], incorporating electronic resistance (R_{el}), ionic resistance (R_{ion}), and R-CPE elements to represent the CAM-catholyte interface, with the charge transfer resistance (R_{ct}) being proportional to the CAM surface area. Fig. 6e shows the calculated resistance values for R_{sol} and R_{int} during both charge and discharge cycles (60 data points). In agreement with the Nyquist plots, R_{sol} and R_{int} exhibit a slight increase during the charge from 2.5 to 3.5 V. These values then stabilise between 3.5 and 3.8 V, followed by a decrease from 3.8 to 4.0 V. However, as the intercalation progresses and the potential decreases from 4.0 to 3.2 V vs. Li^+/Li, the resistance values begin to increase but then remain constant until the end of discharge.

These changes in the R_{int} may result from alterations in the near-surface region of the active material, modifications in the interfacial region of the electrolyte, or the formation of an interlayer [42].

4. Conclusions

Herein, we introduce an advanced solid polymer electrolyte (SPE) composed of a poly(ethylene oxide)/poly(ethylene carbonate) (PEO/PEC) network with dissolved lithium bis(trifluoromethanesulfonyl) imide (LiTFSI), offering superior performance compared to conventional PEO-based electrolytes. The electrolyte was produced using an extrusion process that eliminates organic solvents and liquid components, preventing potential leaching and reducing costs. This method employs polymers with low environmental impact and is scalable for industrial application. Furthermore, an UV-induced crosslinking step was applied to induce crosslinking of the polymer chains, thus enhancing the thermomechanical and electrochemical properties, improving thermal stability, and reducing crystallinity.

Symmetric Li||Li cells assembled with the crosslinked PEO-PEC-UV membrane demonstrated outstanding stripping/plating performance across a current density range of 0.025–0.2 mA cm^{-2} at 40 and 70 °C, with stable cycling for over 600 h at 0.05 mA cm^{-2} and no observable lithium dendrite growth, based on the characterization techniques used. Furthermore, rate capability tests were conducted at both 40 and 70 °C on lab-scale lithium metal polymer cells, assembled with a high-loading LFP-based composite catholyte (up to 10 mg cm^{-2}) and PEO-PEC-UV, demonstrating excellent galvanostatic charge/discharge performance up to C/5 rate. Degradation phenomena were also investigated, revealing that the UV-crosslinking process facilitated the in-*situ* production of liquid ethylene carbonate, which enhanced the electrochemical performance of the resulting electrolyte while being trapped within the polymer matrix. These findings confirm that the combination of dry extrusion and UV-induced crosslinking offers a truly solvent-free, simple, and scalable approach for producing greener and more sustainable SPEs with enhanced thermomechanical and electrochemical properties, suitable for future applications in batteries at near ambient temperature operating conditions.

CRediT authorship contribution statement

Matteo Gastaldi: Writing – review & editing, Writing – original draft, Formal analysis, Data curation, Conceptualization. **Francesco Gambino:** Writing – review & editing, Writing – original draft, Investigation, Formal analysis, Data curation, Conceptualization. **Hamideh Darjazi:** Writing – review & editing, Writing – original draft, Methodology, Investigation, Formal analysis, Data curation, Conceptualization. **Alia Jouhara:** Writing – review & editing. **Samuel Malburet:** Writing – review & editing. **Marco Zanetti:** Writing – review & editing, Formal analysis, Data curation. **Guido Saracco:** Writing – review & editing. **Giuseppe Antonio Elia:** Writing – review & editing, Writing – original draft, Supervision, Methodology, Funding acquisition, Conceptualization. **Claudio Gerbaldi:** Writing – review & editing, Writing – original draft, Supervision, Project administration, Funding acquisition, Formal analysis, Data curation, Conceptualization.

Declaration of competing interest

The authors declare that they have no known competing financial interests or personal relationships that could have appeared to influence

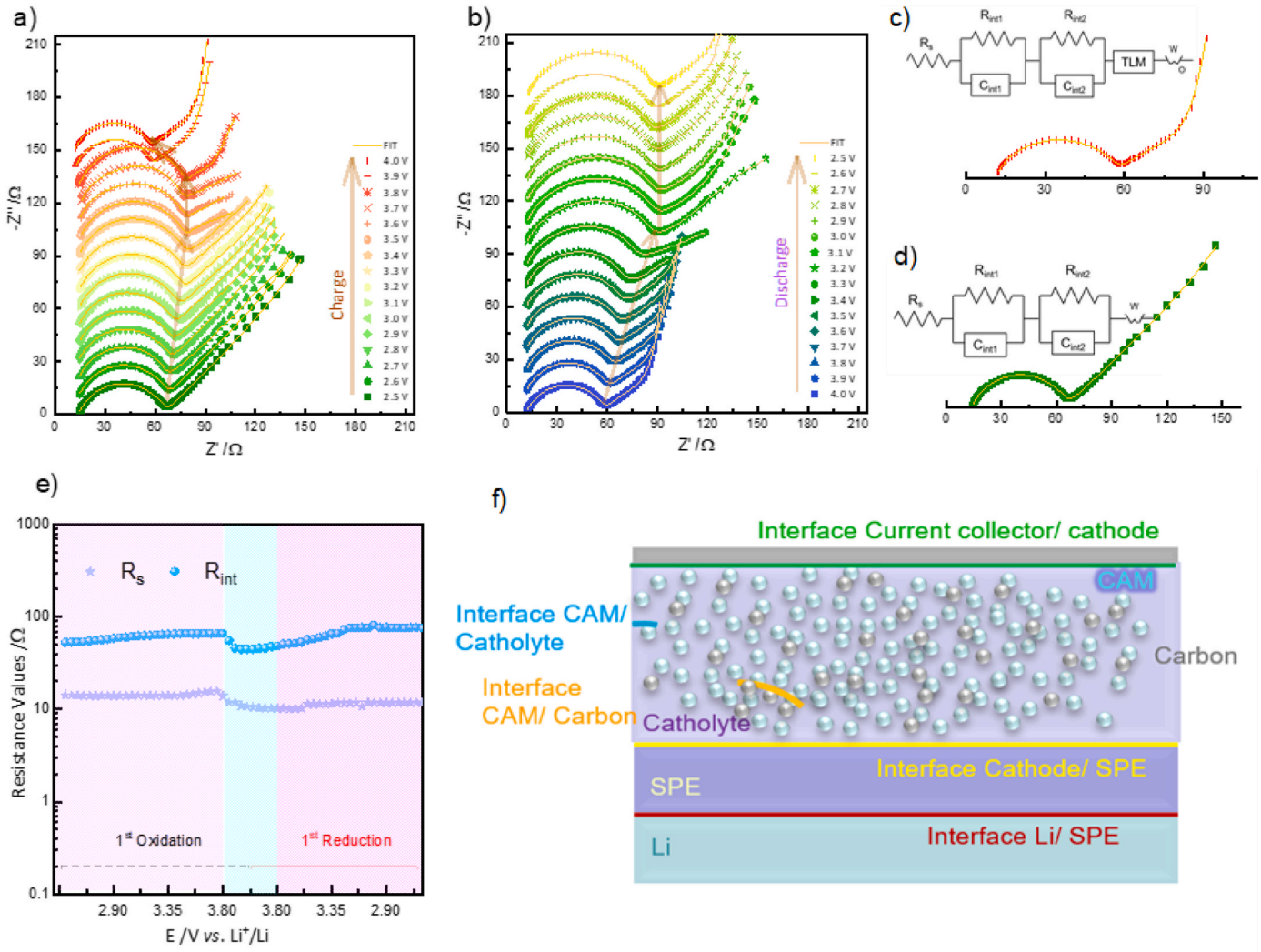

Fig. 6. The corresponding Nyquist plots recorded at selected potentials during the first oxidation (a) and the first reduction (b); the equivalent circuits used to simulate the data (c,d); the fitted resistance values during the first charge and discharge (e); schematic illustration of various interfaces in a Li||PEO-PEC-UV||LFP catholyte cell (f).

the work reported in this paper.

Acknowledgements

The PSIONIC project has received funding from the European Union's Horizon Europe Research and Innovation Programme under Grant Agreement N. 101069703. This study was carried out under the National Recovery and Resilience Plan (NRRP), within the MOST – Sustainable Mobility Center and received funding from the European Union Next-GenerationEU (PIANO NAZIONALE DI RIPRESA E RESILIENZA – PNRR Mission 4, Component 2, Investment 1.4 and D.D. 1033 June 17, 2022 of the Ministero dell'Università e della Ricerca (MUR), CN00000023). This manuscript reflects only the authors' views and opinions, neither the European Union nor the European Commission can be considered responsible for them. The authors acknowledge the program Piano Triennale della Ricerca (PTR) within "Ricerca Sistema Elettrico Nazionale 2025–2027″ funded through contributions to research and development by the Italian Ministry of Economic Development. Prof. Alberto Fina and Dr. Lorenza Maddalena are gratefully acknowledged for their support in DMA measurements. Prof. Claudia Barolo and Dr. Francesca Cardano are thankfully recognized for their support in performing NMR experiments, and Dr. Giovanna Colucci for the DSC experiments.

Appendix A. Supplementary data

Supplementary data to this article can be found online at https://doi.org/10.1016/j.mtener.2025.101947.

Data availability

Data will be made available on request.

References

[1] J. Mindemark, M.J. Lacey, T. Bowden, D. Brandell, Beyond PEO—Alternative host materials for Li+-conducting solid polymer electrolytes, Prog. Polym. Sci. 81 (2018) 114–143, https://doi.org/10.1016/j.progpolymsci.2017.12.004.

[2] Y. He, Y. Dong, L. Qiao, C.M. Costa, S. Lanceros-Méndez, J. Han, W. He, Recent progress in ultra-thin solid polymeric electrolytes for next-generation lithium batteries, Energy Storage Mater. 67 (2024) 103329, https://doi.org/10.1016/j.ensm.2024.103329.

[3] M.A. Cabañero Martínez, N. Boaretto, A.J. Naylor, F. Alcaide, G.D. Salian, F. Palombarini, E. Ayerbe, M. Borras, M. Casas-Cabanas, Are polymer-based electrolytes Ready for high-voltage lithium battery applications? An Overview of degradation Mechanisms and battery performance, Adv. Energy Mater. 12 (2022) 2201264, https://doi.org/10.1002/aenm.202201264.

[4] L. Herbers, J. Minář, S. Stuckenberg, V. Küpers, D. Berghus, S. Nowak, M. Winter, P. Bieker, The influence of polyethylene oxide degradation in polymer-based electrolytes for NMC and lithium metal batteries, Adv. Energy Sustain. Res. 4 (2023) 2300153, https://doi.org/10.1002/aesr.202300153.

[5] B. Guo, Y. Fu, J. Wang, Y. Gong, Y. Zhao, K. Yang, S. Zhou, L. Liu, S. Yang, X. Liu, F. Pan, Strategies and characterization methods for achieving high performance PEO-based solid-state lithium-ion batteries, Chem. Commun. 58 (2022) 8182–8193, https://doi.org/10.1039/D2CC02306G.
[6] Z. Jia, Y. Liu, H. Li, Y. Xiong, Y. Miao, Z. Liu, F. Ren, In-situ polymerized PEO-based solid electrolytes contribute better Li metal batteries: challenges, strategies, and perspectives, J. Energy Chem. 92 (2024) 548–571, https://doi.org/10.1016/j.jechem.2024.01.017.
[7] Q. Han, S. Wang, W. Kong, W. Ren, Y. Liu, H. Wang, Realizing compatibility of high voltage cathode and poly (ethylene oxide) electrolyte in all-solid-state lithium batteries by bilayer electrolyte design, Chem. Eng. J. 454 (2023) 140104, https://doi.org/10.1016/j.cej.2022.140104.
[8] A.M. Elmér, P. Jannasch, Synthesis and characterization of poly(ethylene oxide-co-ethylene carbonate) macromonomers and their use in the preparation of crosslinked polymer electrolytes, J. Polym. Sci. Part Polym. Chem. 44 (2006) 2195–2205, https://doi.org/10.1002/pola.21324.
[9] L. Yue, J. Ma, J. Zhang, J. Zhao, S. Dong, Z. Liu, G. Cui, L. Chen, All solid-state polymer electrolytes for high-performance lithium ion batteries, Energy Storage Mater. 5 (2016) 139–164, https://doi.org/10.1016/j.ensm.2016.07.003.
[10] Q. Guo, F. Xu, L. Shen, Z. Wang, J. Wang, H. He, X. Yao, Poly(ethylene glycol) brush on Li6.4La3Zr1.4Ta0.6O12 towards intimate interfacial compatibility in composite polymer electrolyte for flexible all-solid-state lithium metal batteries, J. Power Sources 498 (2021) 229934, https://doi.org/10.1016/j.jpowsour.2021.229934.
[11] H. Chen, D. Adekoya, L. Hencz, J. Ma, S. Chen, C. Yan, H. Zhao, G. Cui, S. Zhang, Stable Seamless interfaces and Rapid ionic conductivity of Ca–CeO2/LiTFSI/PEO composite electrolyte for high-rate and high-voltage all-solid-state battery, Adv. Energy Mater. 10 (2020) 2000049, https://doi.org/10.1002/aenm.202000049.
[12] J. Li, X. Chen, S. Muhammad, S. Roy, H. Huang, C. Yu, Z. Ullah, Z. Wang, Y. Zhang, K. Wang, B. Guo, Development of solid polymer electrolytes for solid-state lithium battery applications, mater, Today Energy (2024) 101574, https://doi.org/10.1016/j.mtener.2024.101574.
[13] J. Zhu, R. Zhao, J. Zhang, X. Song, J. Liu, N. Xu, H. Zhang, X. Wan, X. Ji, Y. Ma, C. Li, Y. Chen, Long-cycling and High-voltage Solid State Lithium Metal Batteries Enabled by Fluorinated and Crosslinked Polyether Electrolytes, Angew. Chem. Int. Ed. n/a (n.d.) e202400303. https://doi.org/10.1002/anie.202400303.
[14] Y. Zhao, Y. Bai, W. Li, M. An, Y. Bai, G. Chen, Design strategies for polymer electrolytes with ether and carbonate groups for solid-state lithium metal batteries, Chem. Mater. 32 (2020) 6811–6830, https://doi.org/10.1021/acs.chemmater.9b04521.
[15] M. Falco, L. Castro, J.R. Nair, F. Bella, F. Bardé, G. Meligrana, C. Gerbaldi, UV-Cross-Linked composite polymer electrolyte for high-rate, ambient temperature lithium batteries, ACS Appl. Energy Mater. 2 (2019) 1600–1607, https://doi.org/10.1021/acsaem.8b02185.
[16] M. Falco, C. Simari, C. Ferrara, J.R. Nair, G. Meligrana, F. Bella, I. Nicotera, P. Mustarelli, M. Winter, C. Gerbaldi, Understanding the effect of UV-induced cross-linking on the Physicochemical properties of highly performing PEO/LiTFSI-Based polymer electrolytes, Langmuir 35 (2019) 8210–8219, https://doi.org/10.1021/acs.langmuir.9b00041.
[17] R. Khurana, J.L. Schaefer, L.A. Archer, G.W. Coates, Suppression of lithium dendrite growth using cross-Linked polyethylene/poly(ethylene oxide) electrolytes: a new approach for practical lithium-metal polymer batteries, J. Am. Chem. Soc. 136 (2014) 7395–7402, https://doi.org/10.1021/ja502133j.
[18] B. Sun, J. Mindemark, K. Edström, D. Brandell, Polycarbonate-based solid polymer electrolytes for Li-ion batteries, Solid State Ionics 262 (2014) 738–742, https://doi.org/10.1016/j.ssi.2013.08.014.
[19] Z. Wang, L. Shen, S. Deng, P. Cui, X. Yao, 10 μm-thick high-Strength solid polymer electrolytes with excellent interface compatibility for flexible all-solid-state lithium-metal batteries, Adv. Mater. 33 (2021) 2100353, https://doi.org/10.1002/adma.202100353.
[20] Z. Cui, V. Marangon, J. Hassoun, Y. Tominaga, Polycarbonate-based composite polymer electrolytes with Al2O3 enhanced by in situ polymerized electrolyte Interlayers for all-solid-state lithium-metal batteries, J. Power Sources 611 (2024) 234760, https://doi.org/10.1016/j.jpowsour.2024.234760.
[21] N. Soontornnon, K. Kimura, Y. Tominaga, A highly salt concentrated ethylene carbonate-based self-standing copolymer electrolyte for solid-state lithium metal batteries, J. Mater. Chem. A (2024), https://doi.org/10.1039/D4TA03543G.
[22] T. Li, P.K. Panda, C.-T. Hsieh, Y.A. Gandomi, P.-C. Yang, Lithium iron phosphate cathode supported solid lithium batteries with dual composite solid electrolytes enabling high energy density and stable cyclability, J. Energy Storage 81 (2024) 110444, https://doi.org/10.1016/j.est.2024.110444.
[23] A. Buchheit, M. Grünebaum, B. Teßmer, M. Winter, H.-D. Wiemhöfer, Polycarbonate-based lithium salt-containing electrolytes: new Insights into thermal stability, J. Phys. Chem. C 125 (2021) 4371–4378, https://doi.org/10.1021/acs.jpcc.0c09968.
[24] F. Gambino, M. Gastaldi, A. Jouhara, S. Malburet, S. Galliano, N. Cavallini, G. Colucci, M. Zanetti, A. Fina, G.A. Elia, C. Gerbaldi, Formulating PEO-polycarbonate blends as solid polymer electrolytes by solvent-free extrusion, J. Power Sources Adv 30 (2024) 100160, https://doi.org/10.1016/j.powera.2024.100160.
[25] M. Doytcheva, D. Dotcheva, R. Stamenova, A. Orahovats, Ch Tsvetanov, J. Leder, Ultraviolet-induced crosslinking of solid poly(ethylene oxide), J. Appl. Polym. Sci. 64 (1997) 2299–2307, https://doi.org/10.1002/(SICI)1097-4628(19970620)64:12<2299::AID-APP5>3.0.CO;2-G.
[26] L. Porcarelli, C. Gerbaldi, F. Bella, J.R. Nair, Super Soft all-ethylene oxide polymer electrolyte for Safe all-solid lithium batteries, Sci. Rep. 6 (2016) 19892, https://doi.org/10.1038/srep19892.
[27] K. Platen, F. Langer, J. Schwenzel, Influence of Screw design and process parameters on the product quality of PEO:LiTFSI solid electrolytes using solvent-free melt extrusion, Batteries 10 (2024) 183, https://doi.org/10.3390/batteries10060183.
[28] E. Martuscelli, C. Silvestre, M.L. Addonizio, L. Amelino, Phase structure and compatibility studies in poly(ethylene oxide)/poly(methyl methacrylate) blends, Makromol. Chem. 187 (1986) 1557–1571, https://doi.org/10.1002/macp.1986.021870625.
[29] X. Wen, Y. Su, S. Li, W. Ju, D. Wang, Isothermal crystallization kinetics of poly (ethylene oxide)/Poly(ethylene glycol)-g-silica nanocomposites, Polymers 13 (2021) 648, https://doi.org/10.3390/polym13040648.
[30] J. Evans, C.A. Vincent, P.G. Bruce, Electrochemical measurement of transference numbers in polymer electrolytes, Polymer 28 (1987) 2324–2328, https://doi.org/10.1016/0032-3861(87)90394-6.
[31] H. Wang, X. Cui, C. Zhang, H. Gao, W. Du, Y. Chen, Promotion of ionic conductivity of PEO-based solid electrolyte using ultrasonic vibration, Polymers 12 (2020) 1889, https://doi.org/10.3390/polym12091889.
[32] Z. Wang, B. Al Alwan, W. Fawaz, K.Y.S. Ng, Novel PEO-based composite solid electrolytes for All-Solid-State Li-S battery, J. Electroanal. Chem. 954 (2024) 118017, https://doi.org/10.1016/j.jelechem.2023.118017.
[33] Y. Ji, Y.-H. Zhang, F.-N. Shi, L.-N. Zhang, UV-derived double crosslinked PEO-based solid polymer electrolyte for room temperature, J. Colloid Interface Sci. 629 (2023) 492–500, https://doi.org/10.1016/j.jcis.2022.09.089.
[34] Y. Tominaga, V. Nanthana, D. Tohyama, Ionic conduction in poly(ethylene carbonate)-based rubbery electrolytes including lithium salts, Polym. J. 44 (2012) 1155–1158, https://doi.org/10.1038/pj.2012.97.
[35] K. Platen, F. Langer, R. Bayer, R. Hollmann, J. Schwenzel, M. Busse, Influence of molecular weight and lithium bis(trifluoromethanesulfonyl)imide on the thermal processability of poly(ethylene oxide) for solid-state electrolytes, Polymers 15 (2023) 3375, https://doi.org/10.3390/polym15163375.
[36] A. Nishimoto, K. Agehara, N. Furuya, T. Watanabe, M. Watanabe, High ionic conductivity of polyether-based network polymer electrolytes with hyperbranched side chains, Macromolecules 32 (1999) 1541–1548, https://doi.org/10.1021/ma981436q.
[37] M.Z.A. Munshi, B.B. Owens, Ionic transport in poly(ethylene oxide) (PEO)-LiX polymeric solid electrolyte, Polym. J. 20 (1988) 577–586, https://doi.org/10.1295/polymj.20.577.
[38] Z. Chen, Y. Zhang, B. Zhu, J. Wang, J. Hu, J. Zou, Z. Jin, X. Li, Y. Zhang, C. Zhang, Construction of high-performance solid-state electrolytes for lithium metal batteries by UV-curing technology, Polym. Test. 132 (2024) 108386, https://doi.org/10.1016/j.polymertesting.2024.108386.
[39] S. Huo, L. Sheng, W. Xue, L. Wang, H. Xu, H. Zhang, X. He, Challenges of polymer electrolyte with wide electrochemical window for high energy solid-state lithium batteries, InfoMat 5 (2023) e12394, https://doi.org/10.1002/inf2.12394.
[40] E. Quartarone, P. Mustarelli, Electrolytes for solid-state lithium rechargeable batteries: recent advances and perspectives, Chem. Soc. Rev. 40 (2011) 2525–2540, https://doi.org/10.1039/C0CS00081G.
[41] B. Sun, C. Xu, J. Mindemark, T. Gustafsson, K. Edström, D. Brandell, At the polymer electrolyte interfaces: the role of the polymer host in interphase layer formation in Li-batteries, J. Mater. Chem. A 3 (2015) 13994–14000, https://doi.org/10.1039/C5TA02485D.
[42] V. Wurster, C. Engel, H. Graebe, T. Ferber, W. Jaegermann, R. Hausbrand, Characterization of the interfaces in LiFePO4/PEO-LiTFSI composite cathodes and to the adjacent layers, J. Electrochem. Soc. 166 (2019) A5410, https://doi.org/10.1149/2.0621903jes.
[43] H. Darjazi, I. Madinabeitia, M. Zarrabeitia, E. Gonzalo, B. Acebedo, S. Javad Rezvani, F.J. Fernández-Carretero, F. Nobili, A. García-Luis, M.Á. Muñoz-Márquez, LiNi0.5Mn1.5O4 thin films grown by magnetron sputtering under inert gas flow mixtures as high-voltage cathode materials for lithium-ion batteries, Chemelectrochem 10 (2023) e202201004, https://doi.org/10.1002/celc.202201004.
[44] H. Darjazi, S.J. Rezvani, S. Brutti, F. Nobili, Improvement of structural and electrochemical properties of NMC layered cathode material by combined doping and coating, Electrochim. Acta 404 (2022) 139577, https://doi.org/10.1016/j.electacta.2021.139577.
[45] J. Euler, W. Nonnenmacher, Stromverteilung in porösen elektroden, Electrochim. Acta 2 (1960) 268–286, https://doi.org/10.1016/0013-4686(60)80025-4.
[46] L. Balducci, H. Darjazi, E. Gonzalo, R. Cid, F. Bonilla, F. Nobili, Evaluation of electronic–ionic transport properties of a Mg/Zr-modified LiNi0.5Mn1.5O4 cathode for Li-ion batteries, ACS Appl. Mater. Interfaces 15 (2023) 55620–55632, https://doi.org/10.1021/acsami.3c10480.

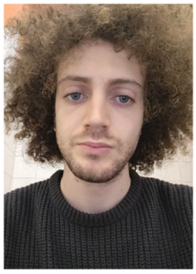

Francesco Gambino completed the master's degree at the University of Turin in October 2020. After a year as a researcher in San Sebastián (Donostia International Physics Center), he began his Ph.D. programme at the Polytechnic University of Turin in 2022. His research focuses on the design and development of advanced polymer electrolytes for lithium batteries.

EDUCATION• PhD Student in Material Science and Technology (Polythecnic of Turin, 2022 – ongoing)• Master Degree in CHEMISTRY (University of Turin, October 2018–October 2020)• Bachelor Degree in CHEMISTRY AND CHEMICAL TECHNOLOGIES (University of Turin, October 2015–October 2018)

Matteo Gastaldi obtained his Ph.D. in Chemistry at the University of Turin in 2022. He is a postdoc researcher at the Polytechnic University of Turin, working on all-solid-state polymer electrolytes for lithium batteries.

EDUCATION• Postdoc researcher at Polytechnic of Turin (2022 – ongoing)• Master Degree in CHEMISTRY (University of Turin, October 2016–October 2018)•Bachelor Degree in CHEMISTRY AND CHEMICAL TECHNOLOGIES (University of Turin, October 2012–October 2016)